Hindawi
Mobile Information Systems
Volume 2017, Article ID 2516035, 16 pages
https://doi.org/10.1155/2017/2516035

Research Article

Outage Analysis and Optimization of SWIPT in Network-Coded Two-Way Relay Networks

Ruihong Jiang,[1] Ke Xiong,[1,2] Yu Zhang,[3] and Zhangdui Zhong[4]

[1]*School of Computer and Information Technology, Beijing Jiaotong University, Beijing 100044, China*
[2]*National Mobile Communications Research Laboratory, Southeast University, Nanjing 210018, China*
[3]*State Grid Energy Research Institute, Beijing 102209, China*
[4]*State Key Lab of Rail Traffic Control and Safety, Beijing Jiaotong University, Beijing 100044, China*

Correspondence should be addressed to Ke Xiong; kxiong@bjtu.edu.cn

Received 2 August 2016; Revised 2 January 2017; Accepted 15 January 2017; Published 22 February 2017

Academic Editor: Yuh-Shyan Chen

This paper investigates the outage performance of simultaneous wireless information and power transfer (SWIPT) in network-coded two-way relay systems, where a relay first harvests energy from the signals transmitted by two sources and then uses the harvested energy to forward the received information to the two sources. We consider two transmission protocols, power splitting two-way relay (PS-TWR) and time switching two-way relay (TS-TWR) protocols. We present two explicit expressions for the system outage probability of the two protocols and further derive approximate expressions for them in high and low SNR cases. To explore the system performance limits, two optimization problems are formulated to minimize the system outage probability. Since the problems are nonconvex and have no known solution methods, a genetic algorithm- (GA-) based algorithm is designed. Numerical and simulation results validate our theoretical analysis. It is shown that, by jointly optimizing the time assignment and SWIPT receiver parameters, a great performance gain can be achieved for both PS-TWR and TS-TWR. Moreover, the optimized PS-TWR always outperforms the optimized TS-TWR in terms of outage performance. Additionally, the effects of parameters including relay location and transmit powers are also discussed, which provide some insights for the SWIPT-enabled two-way relay networks.

1. Introduction

1.1. Background. One of the main challenges in energy-constrained wireless communication networks, for example, the battery-powered wireless sensor networks, is the limited lifetime due to the fixed energy-supplying devices with finite service life. In order to provide a perpetual energy supply to maintain reliable wireless communications, harvesting energy from the surrounding environment is considered as an effective solution [1–9]. Traditional energy harvesting (EH) harvests energy from the external energy sources including solar, wind, and vibration, which are greatly affected and limited by environment or climate, and cannot provide stable energy supply for wireless communication networks [10, 11], while harvesting energy from ambient radio-frequency (RF) signals [12], especially from dedicated radio-frequency radiation, is regarded as a stable and promising energy source for future energy-constrained wireless networks that cannot be offered by conventional battery or grid power-operated wireless communication networks. Because RF signals are independent with the external conditions of the environment and climate and can be easily designed and controlled. Since RF signals can carry energy as well as information at the same time, energy and information can be delivered simultaneously via RF signals, which is known as the simultaneous information and power transfer (SWIPT) advocated in [13–28].

1.2. Related Work. A number of works on SWIPT, thus far, can be found in the literature. In [14], the authors proposed two SWIPT receiver architectures, where energy harvesting and information detection are operated in either power splitting (PS) architecture or time switching (TS) architecture at the receiver, making it possible to realize

SWIPT in practical wireless communication systems. In the past few years, the two receiver architectures have been widely adopted to various wireless communication systems. In [15], the PS and TS architectures were investigated in point-to-point communication systems with SWIPT technology. Later, they were studied in more SWIPT-enabled complex network systems such as nonrelaying two-way transmission systems (see, e.g., [16]), two-hop transmissions (see, e.g., [17]), MIMO communication systems (see, e.g., [18]), and nonregenerative MIMO-OFDM relaying systems (see, e.g., [19]). Besides, SWIPT is also be benefit to the relay networks, so that some existing works focused on the system design and performance analysis for SWIPT-enabled relay networks, see for example, [20–23], where one-way two-hop relay systems with amplify-and-forward (AF) or decode-and-forward (DF) relaying operation were studied.

As is known, the two-way relay network, where two sources exchange their information with a helping relay node, is able to greatly improve system spectral efficiency and throughput by employing some advanced coding technologies such as network coding (NC) [29–31] and the two-way relay transmission has wide applications in various wireless networks, so some recent works began to investigate SWIPT in two-way relay networks; see, for example, [24–28]. Specifically, the work in [24] investigated SWIPT in an AF energy harvesting two-way relay system with TS receiver, where however, only the system bit error rate (BER) performance was analyzed. In [25], the authors studied the outage performance for an asymmetric two-way relaying system with PS receiver architecture, where however, only AF relaying protocol was considered. In [26], the authors analyzed and optimized the system outage performance for two-way relay system, where however, just traditional four-phase two-way EH relay system was considered and NC transmission was not considered. In [27], the authors studied the network-coded two-way relay network from an information theoretical viewpoint, where their goal was to explore the system throughput limit with data rate fairness and the system outage probability was not analyzed, although, in [28], the authors considered SWIPT for a network-coded two-way relay system by using DF relaying and derived the outage probability for the system, where only TS receiver architecture was considered and the time allocation for the two-way relay information transmission was not involved.

1.3. Motivations and Contributions. In this paper, we also study a network-coded two-way relay system with SWIPT and DF relaying operation, where two sources with sufficient energy supply desire to exchange their individual information through an EH relay node. Due to the shadowing of the obstacles like high buildings or the long distance, the direct link between two sources is unavailable.

Compared with previous works, two main differences in our work are stressed as follows. *Firstly*, both TS and PS receiver architectures are took into account in our work, where the power splitting factor for the energy receiver and the time assignment factor for the transmission phases are jointly optimized for PS-TWR, and the time switching factor for the energy receiver and the time assignment factor for the transmission phases are jointly optimized for TS-TWR. *Secondly*, our goal is to explore the system outage performance limits for the PS-TWR and TS-TWR, where network coding is involved in our work.

The main contributions of this paper are summarized as follows. *First*, we derive the closed-form expression of the outage probability for PS-TWR as well as the TS-TWR. *Second*, to explore the system performance limits, two optimization problems are formulated to minimize the outage probability for PS-TWR and TS-TWR, where the power splitting factor for the energy receiver and the time assignment factor for the transmission phases are jointly optimized for PS-TWR, and the time switching factor for the energy receiver and the time assignment factor for the transmission phases are jointly optimized for TS-TWR. *Third*, since two optimization problems are nonconvex and cannot be solved by directly using traditional solution methods, a genetic algorithm (GA)-based scheme is designed to solve them. *Fourth*, in order to achieve simplicity, two approximate expressions of the system outage probabilities of PS-TWR and TS-TWR are derived at the high and low SNR regions, respectively. *Finally*, we provide some numerical and simulation results demonstrate our theoretical analysis associated with the PS-TWR and TS-TWR systems. It is shown that by jointly optimizing the time assignment and the SWIPT receiver parameters, a great performance gain can be achieved for both PS-TWR and TS-TWR. It is also shown that the optimized PS-TWR always outperforms the optimized TS-TWR in terms of outage performance. In addition, the effects of various system parameters including the relay location, the transmit power of the two sources are also discussed, which provide some insights for the SWIPT-enabled two-way relay networks.

1.4. Organization. The rest of the paper is organized as follows. Section 2 describes the system model and the PS-TWR and TS-TWR protocols. Sections 3 and 4 analyze the system outage probability for the two protocols, respectively, where the exact and approximate outage probability expressions of for PS-TWR and TS-TWR are presented. Section 6 formulates two optimization problems to minimize the outage probabilities of PS-TWR and TS-TWR and then designs a GA-based optimization algorithm to solve the problems. Section 7 provides some numerical and simulation results and, finally, Section 8 summarizes the paper with some conclusions.

2. System Model and Protocols

2.1. Network Model. Consider a SWIPT-enabled two-way relay system as shown in Figure 1, where node 1 and node 2, namely, S_1 and S_2, are with sufficient energy supply and desire to exchange their individual information with each other. However, due to the shadowing of some obstacles like the high buildings or the long distance, the direct link between S_1 and S_2 is nonexistent, so that the information exchange between S_1 and S_2 has to be helped by an intermediate node, node 3 (also referred to as node R). It is assumed that node 3 is an energy-selfish/energy contained node, which is not willing to/has no power to help node 1 and node 2 to exchange

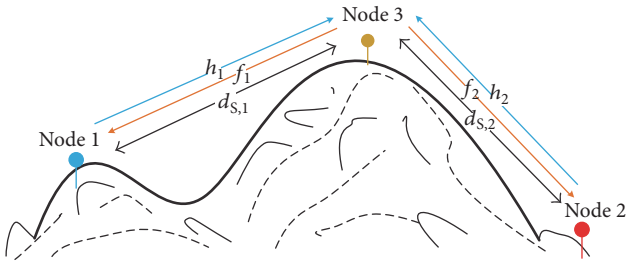

FIGURE 1: System model.

their information. By employing RF-EH technique, node 3 is able to harvest energy from the RF signals transmitted by node 1 and node 2 and then use the harvested energy to help the information transmission. All three nodes are equipped with single antenna. It is worth noting that such an energy-constrained two-way relay model can be applied to many different wireless scenarios, for example, the wireless sensor network (WSN) in a toxic environments and the wireless body area network (WBAN).

Quasi-block fading channel is considered, which means that all channel coefficients associated with the links can be regarded to be constant in each fading block and then change independently from one fading block to the next following Rayleigh distribution. The channel gains of the links from S_i to R and from R to S_i are denoted by h_i and f_i, respectively, and the distances from S_i to R are denoted as $d_{S,i}$, where $i = 1, 2$.

Moreover, S_1 and S_2 have large amount of data to be exchanged and R is with a capacity-limited rechargeable battery buffer, which means that all harvested energy at R in a fading block must be used for the information transmission in the same fading block.

Based on the system mode described above, we shall present the two protocols, PS-TWR and TS-TWR, for the SWIPT-enabled two-way relay system in the following two subsections.

2.2. PS-TWR Protocol. Figure 2(a) illustrates the transmission framework of PS-TWR. Let T be the time period of each fading block. In PS-TWR, T is divided into three parts by the time assignment factors θ_i, that is, $\theta_1 T$, $\theta_2 T$ and $(1-\theta_1-\theta_2)T$, where $0 < \theta_i < 1$ and $0 < \theta_1 + \theta_2 < 1$. In the $\theta_i T$ parts, S_i transmits information to R and, in the $(1-\theta_1-\theta_2)T$ part, R forwards the network-coded information to the two sources.

In first two transmission parts (i.e., source transmission phases), S_i transmits its information to R, where $(1-\rho_i)P_{R,i}$ power is used for the information transmission to R, and the rest $\rho_i P_{R,i}$ power is for energy harvested by R. Here $0 < \rho_i < 1$ denotes the power splitting factor of the energy harvesting receiver, and $P_{R,i}$ is the power of the received signal transmitted from S_i at R, which can be expressed as

$$P_{R,i} = \frac{P_i |h_i|^2}{d_{S,i}^m}, \quad (1)$$

where m is the path loss exponent and P_i is the S_i transmit power.

In the third phase (R forwarding phase), R first decodes the received information transmitted from S_i in first two transmission phases and mixes the two flows of the received information with NC, and then broadcasts the mixed information to S_1 and S_2 using all the harvested energy $\sum_{i=1}^{2} \rho_i P_{R,i}$, simultaneously. Since S_1 and S_2 know their own prior knowledge, they can decode the desired information from the mixed information once they receive the broadcasted information from R.

The receiver architecture of R for PS-TWR is depicted in Figure 2(b), where the received signal y_R is split into two parts for information processing and energy harvesting by a power splitter in $\rho_i : 1-\rho_i$ proportion. So, a part of the received signal $\sqrt{\rho_i} y_R$ is allocated to the EH receiver, the other part $\sqrt{1-\rho_i} y_R$ is for the information receiver. And, the received signal y_R at R is interfered by two noises, $n_{R,a}$ and $n_{R,c}$, where $n_{R,a} \sim \mathcal{CN}(0, \sigma_{R,a}^2)$ is the receiving antenna noise at the relay node R and $\sigma_{R,a}^2$ denotes the noise power. $n_{R,c} \sim \mathcal{CN}(0, \sigma_{R,c}^2)$ is the sampled AWGN introduced by the RF-band to baseband signal conversion at the information receiver as shown in Figure 2(b) and $\sigma_{R,c}^2$ is the noise power.

2.3. TS-TWR Protocol. Figure 3(a) shows the transmission framework of TS-TWR, where T is also divided into three phases by the time assignment factors θ_i as those defined in PS-TWR. However, in TS-TWR, the first two $\theta_i T$ time intervals are further divided into two subphases by the time switching ratio α_i of the TS receiver architecture, where $0 < \alpha_i < 1$ and $i = 1, 2$.

In the first two phases (i.e., source transmission phases), $\alpha_i \theta_i T$ is assigned to R for harvesting energy from the received signals transmitted by S_i and the remaining part $(1-\alpha_i)\theta_i T$ is used for R to receive information from S_i during the first two subphases. In the third phase (R forwarding phase), R first decodes the received information from S_i and mixes the two flows of information with NC, and then broadcasts the mixed information to S_1 and S_2 simultaneously by using all the harvested energy.

The block diagram of TS-TWR the receiver architecture at R is shown in Figure 3(b), where the received RF signal, y_R, at R is input into the energy harvesting receiver in the $\alpha_i \theta_i T$ subphase, and then input into to the information receiver for information decoding during the $(1-\alpha_i)\theta_i T$ subphase. $n_{R,a}$ and $n_{R,c}$ are AWGNs received at R, similar to those defined in PS-TWR.

3. Outage Analysis for PS-TWR

3.1. Exact Expression of the Outage Probability for PS-TWR. As depicted in Figure 2, the individual information is transmitted from S_i to R in the ith source transmission phase, and after the processing of the relay information receiver, the sampled baseband signal $y_{R,i}^{(PS)}$ at R can be given by

$$y_{R,i}^{(PS)} = \frac{1}{\sqrt{d_{S,i}^m}} \sqrt{(1-\rho_i) P_i} h_i x_i + \sqrt{(1-\rho_i)} n_{R,a_i} + n_{R,c_i}, \quad (2)$$

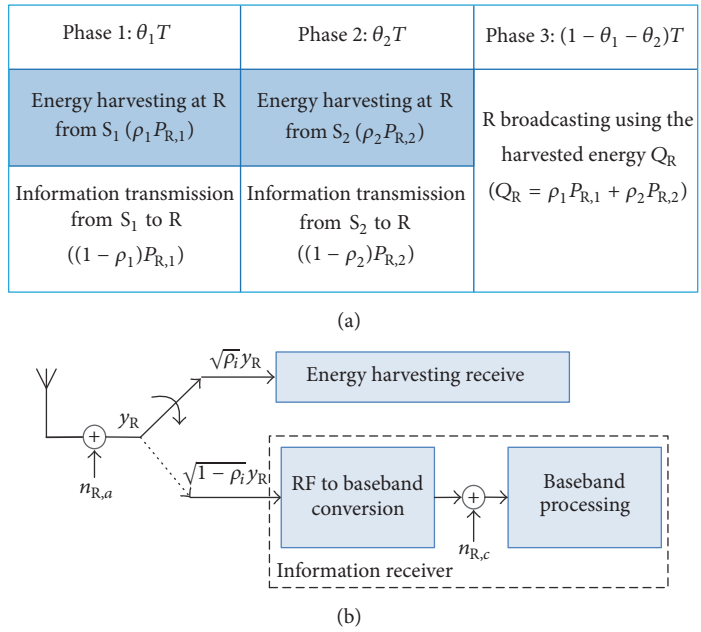

Figure 2: (a) The framework of PS-TWR. (b) Architecture of the relay (R) receiver for PS-TWR.

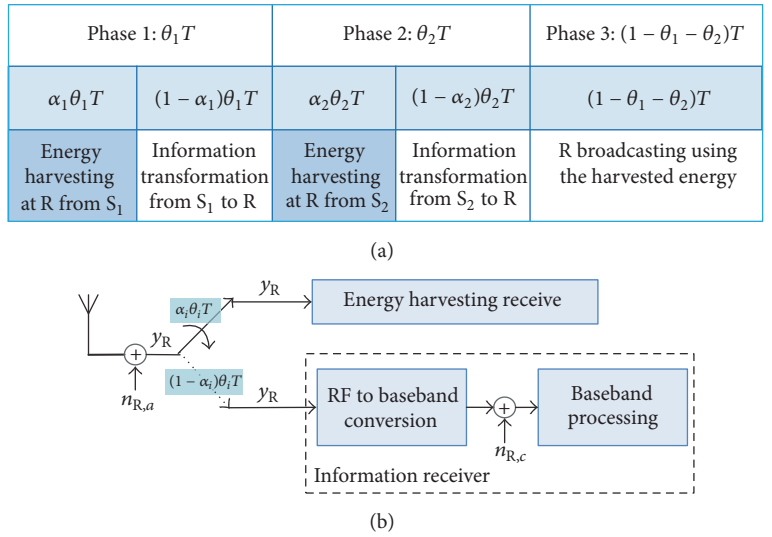

Figure 3: (a) The framework of TS-TWR. (b) Architecture of the relay (R) receiver for TS-TWR.

where x_i is the sampled and normalized information signal from S_i; that is, $E\{|x_i|^2\} = 1$. $E\{\cdot\} = 1$ is the expectation operator and $|\cdot|$ is the absolute value operator. h_i is the channel gain of the link S_i to R. n_{R,a_i} and n_{R,c_i} are the AWGNs with the variances σ^2_{R,a_i} and σ^2_{R,c_i}, respectively. Based on (1), the data rate $R^{(PS)}_{R,i}$ at R from S_i can be given by

$$R^{(PS)}_{R,i} = \theta_i \log\left(1 + \frac{(1-\rho_i)\, P_{R,i}}{\sigma^2_{R,i}}\right) = \theta_i \log\left(1 + \frac{(1-\rho_i)\, P_i\, |h_i|^2}{d^m_{S,i}\sigma^2_{R,i}}\right), \tag{3}$$

where $n_{R,i} \triangleq \sqrt{(1-\rho_i)}n_{R,a_i} + n_{R,c_i}$ with $\sigma^2_{R,i} \triangleq (1-\rho_i)\sigma^2_{R,a_i} + \sigma^2_{R,c_i}$ is the overall AWGNs at R in the first two transmission phases.

Meanwhile, using (1), the RF-band energy $Q^{(PS)}_{R,i}$ harvested by R from S_i at the relay energy harvesting receiver can be given by

$$Q^{(PS)}_{R,i} = \zeta\rho_i P_{R,i}\,(\theta_i T) = \frac{\zeta\rho_i P_i\, |h_i|^2}{d^m_{S,i}}\,(\theta_i T), \tag{4}$$

where $0 < \zeta \leq 1$ is used to describe the energy conversion efficiency, and we assume $\zeta = 1$ in this paper.

After the first two transmission phases, the total energy may be harvested by R from S_1 and S_2 can be expressed as $Q_{R,1}^{(PS)} + Q_{R,2}^{(PS)}$, which is consumed by R to forward the received information in the third relay forwarding phase. As the fact that R communicates with S_i for the time $(1 - \theta_1 - \theta_2)T$ as shown in Figure 2(a) and using $Q_{R,i}^{(PS)}$ in (4), the transmit power of the relay, $Q_R^{(PS)}$, in the third phase can be given by

$$Q_R^{(PS)} = \frac{Q_{R,1}^{(PS)} + Q_{R,2}^{(PS)}}{(1-\theta_1-\theta_2)T} = \frac{1}{1-\theta_1-\theta_2}\sum_{i=1}^{2}\frac{\zeta\rho_i P_i |h_i|^2}{d_{S,i}^m}\theta_i. \quad (5)$$

At the end of R forwarding phase, the received signal $y_{S,i}^{(PS)}$ at S_i from R can be given by

$$y_{S,i}^{(PS)} = \frac{1}{\sqrt{d_{S,i}^m}}\sqrt{Q_R^{(PS)}} f_i x_j + n_{S,a_i} + n_{S,c_i}, \quad (6)$$

where $j = 1, 2$ and $j \neq i$. f_i is the channel gain of the link R to S_i. n_{S,a_i} is the baseband AWGN with variance σ_{S,a_i}^2 and n_{S,c_i} is the sampled AWGN with variance σ_{S,c_i}^2. The achievable date rate at S_i from R can be given by

$$R_{S,i}^{(PS)} = (1-\theta_1-\theta_2)\log\left(1 + \frac{Q_R^{(PS)}|f_i|^2}{d_{S,i}^m \sigma_{S,i}^2}\right), \quad (7)$$

where $n_{S,i} \triangleq n_{S,a_i} + n_{S,c_i}$ with $\sigma_{S,i}^2 \triangleq \sigma_{S,a_i}^2 + \sigma_{S,c_i}^2$.

Due to the impact of channel f_i and the employed NC, the broadcast data rate of R is limited in the third phase. Therefore, the actual achievable broadcast rate, $R_{SR}^{(PS)}$, at S_i from R can be given by

$$\begin{aligned} R_{SR}^{(PS)} &= \min\left(R_{S,1}^{(PS)}, R_{S,2}^{(PS)}\right) \\ &= (1-\theta_1-\theta_2)\log(1+\mathrm{SNR}_{SR}), \end{aligned} \quad (8)$$

where $\mathrm{SNR}_{SR} = \min(Q_R^{(PS)}|f_1|^2/d_{S,1}^m\sigma_{S,1}^2, Q_R^{(PS)}|f_2|^2/d_{S,2}^m\sigma_{S,2}^2)$.

As is known, in traditional one-way relay networks, an outage occurs if either link's rate of two hops falls below the given target rate R_{sr}. Comparatively, the two-way relay networks have two communication tasks which refer to three transmission links: S_1 to R link, S_2 to R link and R forwarding link. Unfortunately, any link's transmission failure can result in system outage. So, we define the system outage probability in terms of the analysis in [32, 33] as follows:

$$P_{out}^{(PS)} = 1 - P_o^{(PS)}, \quad (9)$$

where $P_o^{(PS)} = \Pr[R_{R,1}^{(PS)} \geq R_{sr}]\cdot\Pr[R_{R,2}^{(PS)} \geq R_{sr}]\cdot\Pr[R_{SR}^{(PS)} \geq R_{sr}]$.

Theorem 1. *For PS-TWR protocol, given a predetermined transmission rate R_{sr}, the system outage probability can be calculated as (11) in terms of P_i, θ_i, ρ_i, ζ, and $d_{S,i}$, where*

$$\begin{aligned} a &= \frac{\theta_1}{(1-\theta_1-\theta_2)}\zeta\rho_1 P_1 d_{S,1}^{-m}, \\ b &= \frac{\theta_2}{(1-\theta_1-\theta_2)}\zeta\rho_2 P_2 d_{S,2}^{-m}, \\ c &= \frac{u_1 d_{S,1}^m \sigma_{R,1}^2}{(1-\rho_1)P_1}, \\ d &= \frac{u_2 d_{S,2}^m \sigma_{R,2}^2}{(1-\rho_2)P_2}, \\ u_1 &= 2^{(1/\theta_1)R_{sr}} - 1, \\ u_2 &= 2^{(1/\theta_2)R_{sr}} - 1, \\ u_3 &= 2^{(1/(1-\theta_1-\theta_2))R_{sr}} - 1, \\ z_0 &= d_{S,1}^m \sigma_{S,1}^2 \lambda_{f_1} + d_{S,2}^m \sigma_{S,2}^2 \lambda_{f_2}. \end{aligned} \quad (10)$$

$K_1(\cdot)$ and $K_2(\cdot)$ are the first-order and second-order modified Bessel functions of the second kind, respectively. λ_{h_i} and λ_{f_i} denote the parameter of the exponential random variables $|h_i|^2$ and $|f_i|^2$, respectively.

$$P_{out}^{(PS)} = \begin{cases} 1 - \dfrac{2\lambda_{h_1}\lambda_{h_2}}{a\lambda_{h_2} - b\lambda_{h_1}} e^{-\lambda_{h_1}c - \lambda_{h_2}d}\left(\sqrt{\dfrac{az_0u_3}{\lambda_{h_1}}}K_1\left(2\sqrt{\dfrac{z_0u_3\lambda_{h_1}}{a}}\right) - \sqrt{\dfrac{bz_0u_3}{\lambda_{h_2}}}K_1\left(2\sqrt{\dfrac{z_0u_3\lambda_{h_2}}{b}}\right)\right), & a\lambda_{h_2} \neq b\lambda_{h_1}, \\ 1 - \dfrac{2\lambda_{h_1}z_0u_3}{a} e^{-\lambda_{h_1}c - \lambda_{h_2}d} K_2\left(2\sqrt{\dfrac{z_0u_3\lambda_{h_2}}{b}}\right), & a\lambda_{h_2} = b\lambda_{h_1}. \end{cases} \quad (11)$$

Proof. See the Appendix. □

3.2. Approximate Expressions of the Outage Probability for PS-TWR. Since the theoretical analysis expression of the system outage probability $P_{out}^{(PS)}$ in (11) is complicated with the modified Bessel functions, it is difficult to obtain an analytic solution of $P_{out}^{(PS)}$ by using traditional methods. For the sake of simplicity, the approximate expressions of $P_{out}^{(PS)}$ at extremely high and low SNR regions are formulated in the following theorems.

Theorem 2. *At high SNR region, the approximate expression of the system outage probability $P_{out}^{(PS)}$ in (11) for PS-TWR protocol can be formulated as $P_{PS}^{(high)}$ in*

$$P_{PS}^{(high)} = \begin{cases} 1 - e^{-\lambda_{h_1} c - \lambda_{h_2} d}, & a\lambda_{h_2} \neq b\lambda_{h_1}, \\ 1 - \dfrac{b\lambda_{h_1}}{a\lambda_{h_2}} e^{-\lambda_{h_1} c - \lambda_{h_2} d}, & a\lambda_{h_2} = b\lambda_{h_1}. \end{cases} \tag{12}$$

Proof. If $0 < x \leq \sqrt{v+1}$, the modified Bessel function of the second kind follows from the approximation [34] given by

$$K_v(x) \approx \frac{\Gamma(v)}{2} \left(\frac{2}{x}\right)^v, \quad v > 0, \tag{13}$$

where $\Gamma(v)$ is the Gamma function. Therefore, we can obtain the approximate expressions of $K_1(\cdot)$ and $K_2(\cdot)$ as

$$\begin{aligned} K_1(x) &= \frac{1}{x}, \\ K_2(x) &= \frac{2}{x^2}. \end{aligned} \tag{14}$$

At high SNR region, the variables in $K_1(\cdot)$ and $K_2(\cdot)$ of the system outage probability $P_{\text{out}}^{(\text{PS})}$ are very close to zero with the relatively high variables a and b, which are contained in the denominators of the variables in $K_1(\cdot)$ and $K_2(\cdot)$. Substituting (14) into (11), the approximate expression for $P_{\text{out}}^{(\text{PS})}$ at high SNR region can be calculated as (12). □

Theorem 3. *At low SNR region, the approximate expression of the system outage probability $P_{out}^{(PS)}$ in (11) for PS-TWR protocol can be formulated as $P_{PS}^{(low)}$ in*

$$P_{PS}^{(low)} = \begin{cases} 1 - \dfrac{2\lambda_{h_1}\lambda_{h_2}}{a\lambda_{h_2} - b\lambda_{h_1}} e^{-\lambda_{h_1} c - \lambda_{h_2} d} \left(\sqrt{\dfrac{az_0u_3}{\lambda_{h_1}}} \sqrt{\dfrac{\pi}{4}\sqrt{\dfrac{a}{z_0u_3\lambda_{h_1}}}} e^{-\sqrt{4z_0u_3\lambda_{h_1}/a}} - \sqrt{\dfrac{bz_0u_3}{\lambda_{h_2}}} \sqrt{\dfrac{\pi}{4}\sqrt{\dfrac{b}{z_0u_3\lambda_{h_2}}}} e^{-\sqrt{4z_0u_3\lambda_{h_2}/b}} \right), & a\lambda_{h_2} \neq b\lambda_{h_1}, \\ 1 - \dfrac{2\lambda_{h_1} z_0 u_3}{a} e^{-\lambda_{h_1} c - \lambda_{h_2} d} \sqrt{\dfrac{\pi}{4}\sqrt{\dfrac{b}{z_0u_3\lambda_{h_2}}}} e^{-\sqrt{4z_0u_3\lambda_{h_2}/b}}, & a\lambda_{h_2} = b\lambda_{h_1}. \end{cases} \tag{15}$$

Proof. If $x > |v^2 - 1/4|$, the modified Bessel function of the second kind follows from the approximation [34] as

$$K_v(x) \approx \sqrt{\frac{\pi}{2x}} e^{-x}, \quad v > 0. \tag{16}$$

At low SNR region, the denominators of the variables in $K_1(\cdot)$ and $K_2(\cdot)$ are either a or b, which is relatively low leading to the variables in $K_1(\cdot)$ and $K_2(\cdot)$ of the system outage probability $P_{\text{out}}^{(\text{PS})}$ are very close to infinity. Thus, substituting (16) into (11), the approximate expression of $P_{\text{out}}^{(\text{PS})}$ at low SNR region can be achieved as (15). □

4. Outage Analysis for TS-TWR

4.1. Exact Expression of the Outage Probability for TS-TWR. As shown in Figure 3(b), the RF received signal y_{R} is first sent to the energy harvesting receiver to collect energy by R over the $\alpha_i\theta_i T$ time in the S_i transmission phase. Thus, the received RF signal $y_{\text{R},i}^{(\text{TS})}$ at R for harvesting energy can be given by

$$y_{\text{R},i}^{(\text{TS})} = \frac{1}{\sqrt{d_{\text{S},i}^{\,m}}} \sqrt{P_i} h_i x_i + n_{\text{R},a_i} + n_{\text{R},c_i}, \tag{17}$$

where x_i, m, h_i, n_{R,a_i}, and n_{R,c_i} are defined as (2).

Using (1), the achieved data rate $R_{\text{R},i}^{(\text{TS})}$ at R from S_i in the $(1-\alpha_i)\theta_i T$ subphase can be given by

$$\begin{aligned} R_{\text{R},i}^{(\text{TS})} &= (1-\alpha_i)\,\theta_i \log\left(1 + \frac{P_{\text{R},i}}{\sigma_{\text{R},i}^2}\right) \\ &= (1-\alpha_i)\,\theta_i \log\left(1 + \frac{P_i |h_i|^2}{d_{\text{S},i}^m \sigma_{\text{R},i}^2}\right), \end{aligned} \tag{18}$$

where $n_{\text{R},i} \triangleq n_{\text{R},a_i} + n_{\text{R},c_i}$ with $\sigma_{\text{R},i}^2 \triangleq \sigma_{\text{R},a_i}^2 + \sigma_{\text{R},c_i}^2$.

During the first two transmission phases, the harvested RF-band energy $Q_{\text{R},i}^{(\text{TS})}$ by R from S_i in the $\alpha_i\theta_i T$ subphase can be given by

$$Q_{\text{R},i}^{(\text{TS})} = \frac{\zeta P_i |h_i|^2}{d_{\text{S},i}^m} (\alpha_i \theta_i T), \tag{19}$$

where ζ is the energy conversion efficiency.

At the end of the first two S_i transmission phases, the total energy may be harvested by R from S_1 and S_2 can be expressed as $Q_{\text{R},1}^{(\text{TS})} + Q_{\text{R},2}^{(\text{TS})}$, which is used by R for forwarding the received information to S_1 and S_2 simultaneously in the third relay

forwarding phase. Using $Q_{\mathrm{R},i}^{(\mathrm{TS})}$ in (19), the transmit power of R broadcasting in the third phase can be given by

$$\begin{aligned} Q_{\mathrm{R}}^{(\mathrm{TS})} &= \frac{Q_{\mathrm{R},1}^{(\mathrm{TS})} + Q_{\mathrm{R},2}^{(\mathrm{TS})}}{(1-\theta_1-\theta_2)\,T} \\ &= \frac{1}{1-\theta_1-\theta_2}\sum_{i=1}^{2}\frac{\zeta P_i\,|h_i|^2}{d_{\mathrm{S},i}^m}\,(\alpha_i\theta_i)\,. \end{aligned} \tag{20}$$

At the end of the third R forwarding phase, the sampled received signal at S_i from R can be given by

$$y_{\mathrm{S},i}^{(\mathrm{TS})} = \frac{1}{\sqrt{d_{\mathrm{S},i}^m}}\sqrt{Q_{\mathrm{R}}^{(\mathrm{TS})}}\,f_i x_j + n_{\mathrm{S},a_i} + n_{\mathrm{S},c_i}, \tag{21}$$

where $j = 1, 2$ and $j \neq i$ and f_i, n_{S,a_i}, and n_{S,c_i} are defined as (6).

Finally, the achievable data rate at S_i from R is given by

$$R_{\mathrm{S},i}^{(\mathrm{TS})} = (1-\theta_1-\theta_2)\log\left(1+\frac{Q_{\mathrm{R}}^{(\mathrm{TS})}\,|f_i|^2}{d_{\mathrm{S},i}^m\sigma_{\mathrm{S},i}^2}\right), \tag{22}$$

where $n_{\mathrm{S},i} \triangleq n_{\mathrm{S},a_i} + n_{\mathrm{S},c_i}$ with $\sigma_{\mathrm{S},i}^2 \triangleq \sigma_{\mathrm{S},a_i}^2 + \sigma_{\mathrm{S},c_i}^2$.

In the third relay forwarding phase, the broadcast data rate of R is limited by the effect of the channel f_i and the employed digital NC, so that the actual achievable broadcast rate at S_i from R is

$$\begin{aligned} R_{\mathrm{SR}}^{(\mathrm{TS})} &= \min\left(R_{\mathrm{S},1}^{(\mathrm{TS})}, R_{\mathrm{S},2}^{(\mathrm{TS})}\right) \\ &= (1-\theta_1-\theta_2)\log\left(1+\mathrm{SNR}_{\mathrm{SR}}\right), \end{aligned} \tag{23}$$

where $\mathrm{SNR}_{\mathrm{SR}} = \min(Q_{\mathrm{R}}^{(\mathrm{TS})}|f_1|^2/d_{\mathrm{S},1}^m\sigma_{\mathrm{S},1}^2, Q_{\mathrm{R}}^{(\mathrm{TS})}|f_2|^2/d_{\mathrm{S},2}^m\sigma_{\mathrm{S},2}^2)$.

As described above for PS-TWR, we also define the system outage probability based on the analysis in [32, 33] as follows:

$$P_{\mathrm{out}}^{(\mathrm{TS})} = 1 - P_{\mathrm{o}}^{(\mathrm{TS})}, \tag{24}$$

where $P_{\mathrm{o}}^{(\mathrm{TS})} = \Pr[R_{\mathrm{R},1}^{(\mathrm{TS})} \geq R_{\mathrm{sr}}] \cdot \Pr[R_{\mathrm{R},2}^{(\mathrm{TS})} \geq R_{\mathrm{sr}}] \cdot \Pr[R_{\mathrm{SR}}^{(\mathrm{TS})} \geq R_{\mathrm{sr}}]$.

Theorem 4. *For TS-TWR protocol, given a predetermined transmission rate R_{sr}, the system outage probability also can be calculated as (26) in terms of variants P_i, θ_i, α_i, ζ, and $d_{\mathrm{S},i}$, where*

$$\begin{aligned} a_0 &= \frac{\alpha_1\theta_1}{(1-\theta_1-\theta_2)}\zeta P_1 d_{\mathrm{S},1}^{-m}, \\ b_0 &= \frac{\alpha_2\theta_2}{(1-\theta_1-\theta_2)}\zeta P_2 d_{\mathrm{S},2}^{-m}, \\ c_0 &= \frac{w_1 d_{\mathrm{S},1}^m \sigma_{\mathrm{R},1}^2}{P_1}, \\ d_0 &= \frac{w_2 d_{\mathrm{S},2}^m \sigma_{\mathrm{R},2}^2}{P_2}, \\ w_1 &= 2^{(1/(1-\alpha_1)\theta_1)R_{sr}} - 1, \\ w_2 &= 2^{(1/(1-\alpha_2)\theta_2)R_{sr}} - 1, \\ w_3 &= 2^{(1/(1-\theta_1-\theta_2))R_{sr}} - 1, \\ e_0 &= d_{\mathrm{S},1}^m \sigma_{\mathrm{S},1}^2 \lambda_{f_1} + d_{\mathrm{S},2}^m \sigma_{\mathrm{S},2}^2 \lambda_{f_2}. \end{aligned} \tag{25}$$

$K_1(\cdot)$, $K_2(\cdot)$, λ_{f_1}, and λ_{f_2} are set to be similar to PS-TWR protocol.

$$P_{\mathrm{out}}^{(\mathrm{TS})} = \begin{cases} 1 - \dfrac{2\lambda_{h_1}\lambda_{h_2}}{a_0\lambda_{h_2} - b_0\lambda_{h_1}} e^{-\lambda_{h_1}c_0 - \lambda_{h_2}d_0}\left(\sqrt{\dfrac{a_0 e_0 w_3}{\lambda_{h_1}}}K_1\left(2\sqrt{\dfrac{e_0 w_3 \lambda_{h_1}}{a_0}}\right) - \sqrt{\dfrac{b_0 e_0 w_3}{\lambda_{h_2}}}K_1\left(2\sqrt{\dfrac{e_0 w_3 \lambda_{h_2}}{b_0}}\right)\right), & a_0\lambda_{h_2} \neq b_0\lambda_{h_1}, \\ 1 - \dfrac{2\lambda_{h_1} e_0 w_3}{a_0} e^{-\lambda_{h_1}c_0 - \lambda_{h_2}d_0} K_2\left(2\sqrt{\dfrac{e_0 w_3 \lambda_{h_2}}{b_0}}\right), & a_0\lambda_{h_2} = b_0\lambda_{h_1}. \end{cases} \tag{26}$$

Proof. The detailed derivation of the system outage probability $P_{\mathrm{out}}^{(\mathrm{TS})}$ for TS-TWR is skipped here, because it follows the same steps as given in the Appendix. □

4.2. Approximating Expressions of the Outage Probability for TS-TWR. Due to the theoretical analysis expression of the system outage probability $P_{\mathrm{out}}^{(\mathrm{TS})}$ in (26) is complicated containing the modified Bessel functions, it is difficult to obtain an analytic solution of $P_{\mathrm{out}}^{(\mathrm{TS})}$ by using traditional methods. For the sake of simplicity, the approximate expressions of $P_{\mathrm{out}}^{(\mathrm{TS})}$ at extremely high and low SNR regions are formulated in the following theorems.

Theorem 5. *For TS-TWR protocol, the approximate expression of the system outage probability $P_{out}^{(TS)}$ in (26) at high SNR region can be formulated as $P_{TS}^{(high)}$ in*

$$P_{TS}^{(high)} = \begin{cases} 1 - e^{-\lambda_{h_1}c_0 - \lambda_{h_2}d_0}, & a_0\lambda_{h_2} \neq b_0\lambda_{h_1}, \\ 1 - \dfrac{b_0\lambda_{h_1}}{a_0\lambda_{h_2}} e^{-\lambda_{h_1}c_0 - \lambda_{h_2}d_0}, & a_0\lambda_{h_2} = b_0\lambda_{h_1}. \end{cases} \tag{27}$$

Proof. The detailed derivation of $P_{\mathrm{TS}}^{(\mathrm{high})}$ for TS-TWR protocol is omitted here because it follows the same steps as given in Theorem 2 for PS-TWR protocol. □

Theorem 6. *For TS-TWR protocol, the approximate expression of the system outage probability $P_{out}^{(TS)}$ in (26) at low SNR region can be formulated as $P_{TS}^{(low)}$ in*

$$P_{TS}^{(low)} = \begin{cases} 1 - \dfrac{2\lambda_{h_1}\lambda_{h_2}}{a_0\lambda_{h_2} - b_0\lambda_{h_1}} e^{-\lambda_{h_1}c_0 - \lambda_{h_2}d_0} \left(\sqrt{\dfrac{a_0 e_0 w_3}{\lambda_{h_1}}} \sqrt{\dfrac{\pi}{4}} \sqrt{\dfrac{a_0}{e_0 w_3 \lambda_{h_1}}} e^{-\sqrt{4e_0 w_3 \lambda_{h_1}/a_0}} - \sqrt{\dfrac{b_0 e_0 w_3}{\lambda_{h_2}}} \sqrt{\dfrac{\pi}{4}} \sqrt{\dfrac{b_0}{e_0 w_3 \lambda_{h_2}}} e^{-\sqrt{4e_0 w_3 \lambda_{h_2}/b_0}} \right), & a_0\lambda_{h_2} \neq b_0\lambda_{h_1}, \\ 1 - \dfrac{2\lambda_{h_1} e_0 w_3}{a_0} e^{-\lambda_{h_1}c_0 - \lambda_{h_2}d_0} \sqrt{\dfrac{\pi}{4}} \sqrt{\dfrac{b_0}{e_0 w_3 \lambda_{h_2}}} e^{-\sqrt{4e_0 w_3 \lambda_{h_2}/b_0}}, & a_0\lambda_{h_2} = b_0\lambda_{h_1}. \end{cases} \quad (28)$$

Proof. The detailed derivation of $P_{\mathrm{TS}}^{(\mathrm{low})}$ for TS-TWR protocol is also omitted here because it follows the same steps as given in Theorem 3 for PS-TWR protocol. □

5. Theoretical Comparison of PS-TWR and TS-TWR

As mentioned previously, it can be obtained that the expressions of the harvested RF energy $Q_{\mathrm{R},i}^{(\mathrm{PS/TS})}$ by R in the first two phases and the corresponding transmit power of the relay broadcasting $Q_{\mathrm{R}}^{(\mathrm{PS/TS})}$ in the third phase in PS-TWR and TS-TWR systems, respectively. In order to compare the two systems, we list the terms $Q_{\mathrm{R}}^{(\mathrm{PS/TS})}$, that is, (5) and (20), in Table 1 with the only difference ρ_i and α_i. For the two systems, PS-TWR and TS-TWR, the system outage probabilities can be given by (9) and (24), respectively. Defining $P_{\mathrm{o1}}^{(\mathrm{PS/TS})} = \Pr[R_{\mathrm{R},1}^{(\mathrm{PS/TS})} \geq R_{\mathrm{sr}}]$, $P_{\mathrm{o2}}^{(\mathrm{PS/TS})} = \Pr[R_{\mathrm{R},2}^{(\mathrm{PS/TS})} \geq R_{\mathrm{sr}}]$ and $P_{\mathrm{o3}}^{(\mathrm{PS/TS})} = \Pr[R_{\mathrm{SR}}^{(\mathrm{PS/TS})} \geq R_{\mathrm{sr}}]$, the system outage probabilities can be rewritten as $P_{\mathrm{out}}^{(\mathrm{PS})} = 1 - P_{\mathrm{o1}}^{(\mathrm{PS})} P_{\mathrm{o2}}^{(\mathrm{PS})} P_{\mathrm{o3}}^{(\mathrm{PS})}$ for PS-TWR, and for TS-TWR, it is $P_{\mathrm{out}}^{(\mathrm{TS})} = 1 - P_{\mathrm{o1}}^{(\mathrm{TS})} P_{\mathrm{o2}}^{(\mathrm{TS})} P_{\mathrm{o3}}^{(\mathrm{TS})}$, as shown in Table 1. Moreover, for PS-TWR, $P_{\mathrm{o1}}^{(\mathrm{PS})} = e^{-\lambda_{h,1}c}$, $P_{\mathrm{o2}}^{(\mathrm{PS})} = e^{-\lambda_{h,2}d}$, and for TS-TWR, $P_{\mathrm{o1}}^{(\mathrm{TS})} = e^{-\lambda_{h,1}c_0}$, $P_{\mathrm{o2}}^{(\mathrm{TS})} = e^{-\lambda_{h,2}d_0}$. And the analysis of $P_{\mathrm{o3}}^{((\mathrm{PS/TS}))}$ can be found in the Appendix in terms of variables a, b, u_3, z_0 or a_0, b_0, w_3, e_0, so that the whole system outage probabilities for the two systems can be obtained as shown in Table 1.

From Table 1, as $0 < \rho_i, \alpha_i, \theta_i < 1$, it can be obtained that $c < c_0$, $d < d_0$ with $u_1 < w_1$, $u_2 < w_2$. Thus, $P_{\mathrm{o1}}^{(\mathrm{PS})} > P_{\mathrm{o1}}^{(\mathrm{TS})}$ and $P_{\mathrm{o2}}^{(\mathrm{PS})} > P_{\mathrm{o2}}^{(\mathrm{TS})}$ with the properties of function $f(x) = e^{-x}$, that is, $P_{\mathrm{o1}}^{(\mathrm{PS})} P_{\mathrm{o2}}^{(\mathrm{PS})} > P_{\mathrm{o1}}^{(\mathrm{TS})} P_{\mathrm{o2}}^{(\mathrm{TS})}$.

Further, we discuss the system outage probabilities for PS-TWR and TS-TWR by the following cases on ρ_i, α_i.

Case 1 ($\rho_i = \alpha_i$). In this case, it can be observed that $a = a_0, b = b_0$, $u_3 = w_3$, and $z_0 = e_0$ with the same scenarios for PS-TWR and TS-TWR, which results in the same outage probabilities in the third phase of the two systems; that is, $P_{\mathrm{o3}}^{(\mathrm{PS})} = P_{\mathrm{o3}}^{(\mathrm{TS})}$. In other words, the whole system outage probabilities for PS-TWR and TS-TWR are determined by the outage probabilities of the first two phases, that is, $P_{\mathrm{o1}}^{(\mathrm{PS})}, P_{\mathrm{o2}}^{(\mathrm{PS})}, P_{\mathrm{o1}}^{(\mathrm{TS})}, P_{\mathrm{o2}}^{(\mathrm{TS})}$, in terms of c, d, c_0, d_0, as shown in Table 1. Because $P_{\mathrm{o1}}^{(\mathrm{PS})} P_{\mathrm{o2}}^{(\mathrm{PS})} > P_{\mathrm{o1}}^{(\mathrm{TS})} P_{\mathrm{o2}}^{(\mathrm{TS})}$, we have that $P_{\mathrm{out}}^{(\mathrm{PS})} = 1 - P_{\mathrm{o1}}^{(\mathrm{PS})} P_{\mathrm{o2}}^{(\mathrm{PS})} P_{\mathrm{o3}}^{(\mathrm{PS})} < P_{\mathrm{out}}^{(\mathrm{TS})} = 1 - P_{\mathrm{o1}}^{(\mathrm{TS})} P_{\mathrm{o2}}^{(\mathrm{TS})} P_{\mathrm{o3}}^{(\mathrm{TS})}$. Therefore, in Case 1, the system outage probability for PS-TWR outperforms that for TS-TWR.

Case 2 ($\rho_i < \alpha_i$). In this case, $a < a_0, b < b_0, u_3 = w_3$, and $z_0 = e_0$, so $P_{\mathrm{o3}}^{(\mathrm{PS})} > P_{\mathrm{o3}}^{(\mathrm{TS})}$. Moreover, since $P_{\mathrm{o1}}^{(\mathrm{PS})} P_{\mathrm{o2}}^{(\mathrm{PS})} > P_{\mathrm{o1}}^{(\mathrm{TS})} P_{\mathrm{o2}}^{(\mathrm{TS})}$, $P_{\mathrm{out}}^{(\mathrm{PS})} = 1 - P_{\mathrm{o1}}^{(\mathrm{PS})} P_{\mathrm{o2}}^{(\mathrm{PS})} P_{\mathrm{o3}}^{(\mathrm{PS})} < P_{\mathrm{out}}^{(\mathrm{TS})} = 1 - P_{\mathrm{o1}}^{(\mathrm{TS})} P_{\mathrm{o2}}^{(\mathrm{TS})} P_{\mathrm{o3}}^{(\mathrm{TS})}$. Therefore, in Case 2, the system outage probability for PS-TWR is lower than that for TS-TWR.

Case 3 ($\rho_i > \alpha_i$). In this case, $a > a_0, b > b_0, u_3 = w_3$, and $z_0 = e_0$, so $P_{\mathrm{o3}}^{(\mathrm{PS})} < P_{\mathrm{o3}}^{(\mathrm{TS})}$. However, $P_{\mathrm{o1}}^{(\mathrm{PS})} P_{\mathrm{o2}}^{(\mathrm{PS})} > P_{\mathrm{o1}}^{(\mathrm{TS})} P_{\mathrm{o2}}^{(\mathrm{TS})}$, the system outage of the two systems are difficult to compare theoretically. Thus, we compare them via numerical results in Section 7.

Based on the above analysis, it can be also achieved that the approximating outage probabilities of TS-TWR are higher than that of PS-TWR even at high and low SNR regions.

6. GA-Based Algorithm for Solving the Optimization Problems

6.1. Optimization Problem Formulation for PS-TWR. From the description in Section 3, it can be seen that for PS-TWR, the transmit power P_i of S_i and all channel parameters are known, while the rest parameters such as the conversion efficiency ζ for the energy harvesting, the power splitting factor ρ_i, the time assignment factor θ_i and the distance $d_{\mathrm{S},i}$ between S_1 and S_2 are all required to be determined and configured. Besides, all the parameters maybe effect on the system outage performance so that jointly designing them for achieving the minimal system outage probability is meaningful and necessary. In this subsection, we formulate an optimization problem to minimize the outage performance of PS-TWR by jointly optimizing ρ_i and θ_i, which can be expressed as

$$\begin{aligned} \min_{\rho=[\rho_1,\rho_2];\theta=[\theta_1,\theta_2]} \quad & P_{\mathrm{out}}^{(\mathrm{PS})} \\ \text{s.t.} \quad & 0 < \rho_i < 1, \\ & 0 < \theta_i < 1, \\ & 0 < \theta_1 + \theta_2 < 1. \end{aligned} \quad (29)$$

Table 1: PS-TWR versus TS-TWR.

Items	PS-TWR	TS-TWR
$Q_{\mathrm{R}}^{(\mathrm{PS/TS})}$	$\frac{1}{1-\theta_1-\theta_2}\sum_{i=1}^{2}\frac{\zeta P_i \lvert h_i\rvert^2}{d_{\mathrm{S},i}^m}(\rho_i\theta_i)$	$\frac{1}{1-\theta_1-\theta_2}\sum_{i=1}^{2}\frac{\zeta P_i \lvert h_i\rvert^2}{d_{\mathrm{S},i}^m}(\alpha_i\theta_i)$
$P_{\mathrm{out}}^{(\mathrm{PS/TS})}$	$1-P_{\mathrm{o1}}^{\mathrm{PS}}P_{\mathrm{o2}}^{\mathrm{PS}}P_{\mathrm{o3}}^{\mathrm{PS}}=1-e^{-\lambda_{h_1}c-\lambda_{h_2}d}P_{\mathrm{o3}}^{(\mathrm{PS})}$	$1-P_{\mathrm{o1}}^{\mathrm{TS}}P_{\mathrm{o2}}^{\mathrm{TS}}P_{\mathrm{o3}}^{\mathrm{TS}}=1-e^{-\lambda_{h_1}c_0-\lambda_{h_2}d_0}P_{\mathrm{o3}}^{(\mathrm{TS})}$
Variables	$a=\frac{(\rho_1\theta_1)}{1-\theta_1-\theta_2}\zeta P_1 d_{\mathrm{S},1}^{-m}$ $b=\frac{(\rho_2\theta_2)}{1-\theta_1-\theta_2}\zeta P_2 d_{\mathrm{S},2}^{-m}$ $c=\frac{u_1 d_{\mathrm{S},1}^m\sigma_{\mathrm{R},1}^2}{(1-\rho_1)P_1}$ $d=\frac{u_2 d_{\mathrm{S},2}^m\sigma_{\mathrm{R},2}^2}{(1-\rho_1)P_2}$ $u_1=2^{(1/\theta_1)R_{\mathrm{sr}}}-1$ $u_2=2^{(1/\theta_2)R_{\mathrm{sr}}}-1$ $u_3=2^{(1/(1-\theta_1-\theta_2))R_{\mathrm{sr}}}-1$ $z_0=\left(d_{\mathrm{S},1}^m\sigma_{\mathrm{S},1}^2\lambda_{f_1}+d_{\mathrm{S},2}^m\sigma_{\mathrm{S},2}^2\lambda_{f_2}\right)$	$a_0=\frac{(\alpha_1\theta_1)}{1-\theta_1-\theta_2}\zeta P_1 d_{\mathrm{S},1}^{-m}$ $b_0=\frac{(\alpha_2\theta_2)}{1-\theta_1-\theta_2}\zeta P_2 d_{\mathrm{S},2}^{-m}$ $c_0=\frac{w_1 d_{\mathrm{S},1}^m\sigma_{\mathrm{R},1}^2}{P_1}$ $d_0=\frac{w_2 d_{\mathrm{S},2}^m\sigma_{\mathrm{R},2}^2}{P_2}$ $w_1=2^{(1/(1-\alpha_1)\theta_1)R_{\mathrm{sr}}}-1$ $w_2=2^{(1/(1-\alpha_2)\theta_2)R_{\mathrm{sr}}}-1$ $w_3=2^{(1/(1-\theta_1-\theta_2))R_{\mathrm{sr}}}-1$ $e_0=\left(d_{\mathrm{S},1}^m\sigma_{\mathrm{S},1}^2\lambda_{f_1}+d_{\mathrm{S},2}^m\sigma_{\mathrm{S},2}^2\lambda_{f_2}\right)$

6.2. Optimization Problem Formulation for TS-TWR. For TS-TWR protocol, we also formulate an optimization problem to explore its minimal outage probability by jointly optimizing the time switching factor α_i of the energy receiver and the time assignment factor θ_i. The optimization problem can be expressed by

$$\begin{aligned}\min_{\theta=[\theta_1,\theta_2];\alpha=[\alpha_1,\alpha_2]}\quad & P_{\mathrm{out}}^{(\mathrm{TS})}\\ \text{s.t.}\quad & 0<\alpha_i<1,\\ & 0<\theta_i<1,\\ & 0<\theta_1+\theta_2<1.\end{aligned}\tag{30}$$

6.3. GA-Based Algorithm. Since both problems in (29) and (30) are nonconvex and not easy to derive closed-form solutions by using conventional solution methods, to solve the two problems, we present a GA-based algorithm as follows.

GA-based algorithm is a metaheuristic, which iteratively refines an initial population of candidate solution until some termination criterions are satisfied; it starts with randomly creating an initial population of individuals, which is a group of chromosomes. Then each individual is evaluated using a fitness function and a fitness value is allocated to each individual indicating how to close a candidate solution is to an ideal solution. Based on the survival of the fittest, individuals with better fitness will be selected for evolution, or abandoned. The common genetic operations are selection, crossover and mutation. Selection is used to select parents to create new offsprings including tournament selection, roulette wheel selection and rank selection. Crossover varies the programming of an individual or individuals from one generation to the next including one-point crossover, two-point crossover, and "cut and splice." Mutation causes a certain level of an organism's genes to change at a certain probability so that the problem of local extreme value can be avoided with proper perturbation introduced by mutation including mut, mutate, and mutbga. Finally, once the termination conditions are satisfied, the process of evolution is stopped [26, 28, 35].

In our work, the main steps of GA-based algorithm are simply described in Algorithm 1 for PS-TWR and TS-TWR.

7. Numerical Results

In this section, some simulation and numerical results are presented to validate our analysis and discuss the performance of the proposed PS-TWR and TS-TWR protocols. In our simulations, we consider a typical three-node relaying network as shown in Figure 4, in which there is an obstacle between S_1 and S_2. The relay R is located on the top of the obstacle to help the information exchanging between S_1 and S_2. Note that the height of the obstacle is varied according to the different environment conditions.

The distance between S_1 and S_1 is denoted as $d_{\mathrm{S,S}}$, which is regarded as a reference distance. The variable, $0<\varphi<1$, is applied to describe the ratio of the distance from S_1 to the obstacle. And h is the height of the obstacle, where we define it as the setting height of R. Therefore, the distance from S_i to R can be given by

$$\begin{aligned}d_{\mathrm{S},1}&=\sqrt{\left(\varphi d_{\mathrm{S,S}}\right)^2+h^2},\\ d_{\mathrm{S},2}&=\sqrt{\left(\left(1-\varphi\right)d_{\mathrm{S,S}}\right)^2+h^2}.\end{aligned}\tag{31}$$

Note that, if $h=0$, R is located on the direct line S_1-to-S_2, which is generally considered as a model to discuss that R is moving along the direct S_1-to-S_2 link. If $h\neq 0$, R is located on the top of the obstacle hindering S_1 and S_2 communication, which is common in our real life as shown in Figure 1. The power spectral density of the receiving noise at S_i is set to be −100 dBm as well as at R. Besides, the path loss effect is also considered, where the path loss exponent is 3, and the distance of the direct S_1-to-S_2 link, $d_{\mathrm{S,S}}$, is set to be 100 m.

Step 1. Setting the population size: N, selection rate: P_s, crossover rate: P_c, mutation rate: P_m;
Step 2. Population initialization: coding to individuals (ρ_i, θ_i) for PS-TWR or (α_i, θ_i) for TS-TWR randomly generates N chromosomes to from the initial population: $Chrom = crtbp(\cdot)$, setting generations count: $gen = 0$;
Step 3. Fitness evaluation: evaluating individuals (ρ_i, θ_i) fitness by the objective function in (11) for PS-TWR or (26) for TS-TWR: $FitnV = ranking(P_{\text{out}}(\cdot))$;
Step 4. If the end condition is met, algorithm ends. Otherwise, go to *Step 3*.
Step 5. Selection: $select('rws', Chrom, FitnV, P_s)$;
Step 6. Crossover: $recombin('xovsp', P_c)$;
Step 7. Mutation: $Smut(SelCh, P_m)$;
Step 8. Inserting offsprings to parent produces a new population: $reins(\cdot)$. $gen = gen + 1$, go to *Step 2*.

Algorithm 1: GA-based algorithm for PS-TWR and TS-TWR.

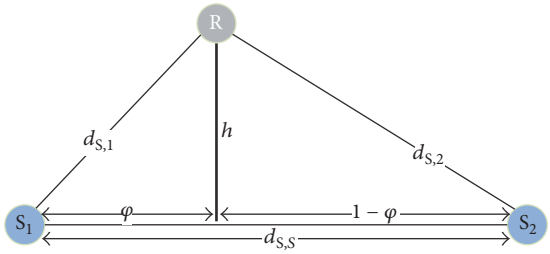

Figure 4: The graph of experimental scene for PS-TWR and TS-TWR.

Table 2: Five scenarios for PS-TWR.

Number	Scenarios
1	Fixed $\rho_1 = \rho_2 = 1/2, \theta_1 = \theta_2 = 1/3$
2	Optimal ρ, with $\theta_1 = \theta_2 = 1/3$ and $\rho_1 = \rho_2 = \rho$
3	Optimal ρ, θ_1, θ_2 with $\rho_1 = \rho_2 = \rho$
4	Optimal ρ_1, ρ_2, with $\theta_1 = \theta_2 = 1/3$
5	Optimal $\rho_1, \rho_2, \theta_1, \theta_2$

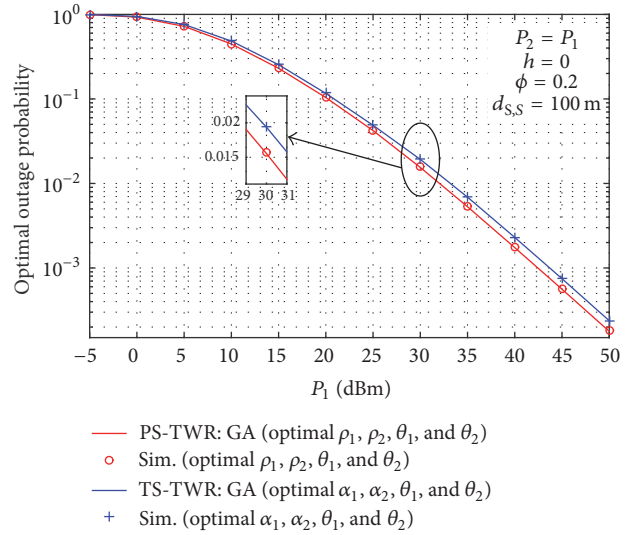

Figure 5: System outage probability: numerical versus simulation for PS-TWR and TS-TWR with $P_2 = P_1$, $h = 0$, $\varphi = 0.2$, and $d_{S,S} = 100$ m.

Table 3: Five scenarios for TS-TWR.

Number	Scenarios
1	Fixed $\alpha_1 = \alpha_2 = 1/2, \theta_1 = \theta_2 = 1/3$
2	Optimal α, with $\theta_1 = \theta_2 = 1/3$ and $\alpha_1 = \alpha_2 = \alpha$
3	Optimal $\alpha, \theta_1, \theta_2$ with $\alpha_1 = \alpha_2 = \alpha$
4	Optimal α_1, α_2, with $\theta_1 = \theta_2 = 1/3$
5	Optimal $\alpha_1, \alpha_2, \theta_1, \theta_2$

Based on the simulation network model as presented in Figure 4, we consider five different system configurations (or scenarios) for comparison, as shown in Table 2 for PS-TWR and Table 3 for TS-TWR, respectively. Besides, unless specifically stated, we set $R_{\text{sr}} = 1$ bit/sec/Hz, $\zeta = 1$. For simplicity, all the mean values of the exponential random variables $|h_1|^2$, $|h_2|^2$, $|f_1|^2$ and $|f_2|^2$ are set to be 1.

7.1. Verification of Analytical Results. In this subsection, some simulation results are presented to verify our analytical expressions of the system outage probability and the effectiveness of our designed GA-based algorithm, where the Monte Carlo simulation is adopted by using up to 10^5 simples. In Figure 5, we present the system outage performances of both PS-TWR and TS-TWR versus the available S_1 transmit power P_1 for $\varphi = 0.2$ with $P_2 = P_1$ and $h = 0$ based on the 5th scenario as shown in Tables 2 and 3, respectively.

From Figure 5, firstly, it can be seen that the numerical and simulation results match very well for PS-TWR and TS-TWR, which demonstrates our theoretical analysis for the system outage probability and GA-based algorithm. Moreover, it shows that the two protocols can achieve lower system outage probability with the increment of P_1. The reason is that more P_1 will lead to higher SNR. It is also shown that the system outage performance of TS-TWR is higher than that of PS-TWR, because in the same channel conditions, the system outage performances of PS-TWR and TS-TWR rely on the information received and energy harvested by R. To well balance information transmission and energy harvesting, for TS-TWR, except for the system transmission time assignment and the power allocation, information

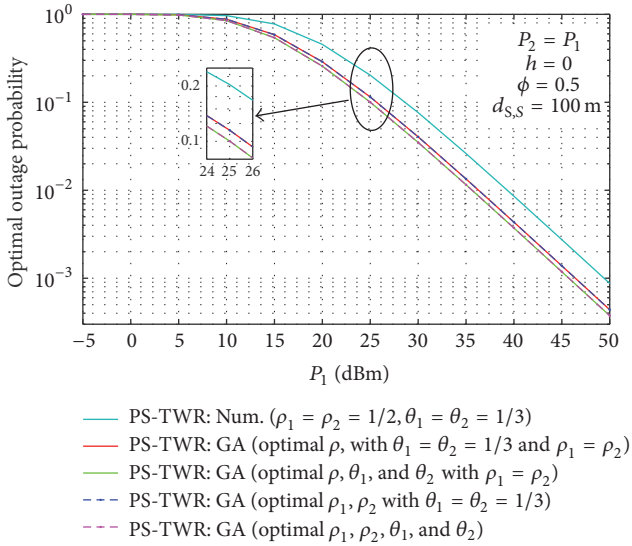

FIGURE 6: System outage probability versus P_1 for PS-TWR with $P_2 = P_1$, $h = 0$, $\varphi = 0.5$, and $d_{S,S} = 100$ m.

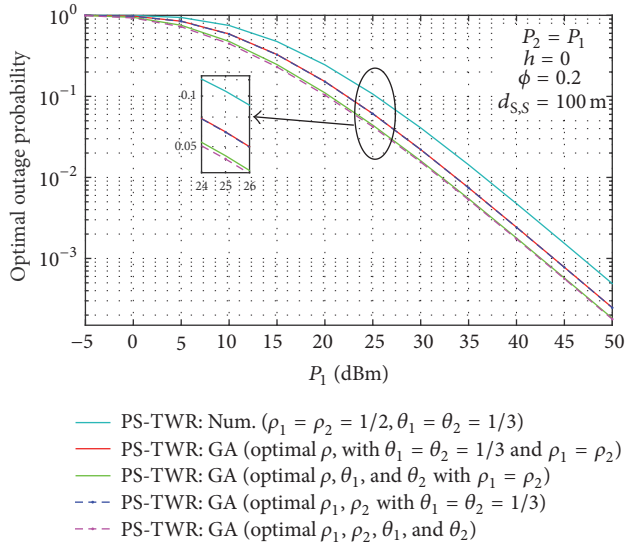

FIGURE 7: System outage probability versus P_1 for PS-TWR with $P_2 = P_1$, $h = 0$, $\varphi = 0.2$, and $d_{S,S} = 100$ m.

decoding and energy harvesting processed by TS receiver at R are sequenced over the S_i transmission phase with the different time switching factor. But for PS-TWR, except for the system transmission time assignment and the power allocation, information decoding and energy harvesting are indeed processed simultaneously by PS receiver at R over the S_i transmission phase with the different power splitting factor. PS-TWR comparing with TS-TWR is more intelligent to allocate the system resources, so it may greatly improve the system outage performance compared with TS-TWR as shown in Figure 5.

7.2. Effect of S_i's Transmit Power on System Performance. Figures 6 and 7 depict the system outage performances of both PS-TWR and TS-TWR versus P_1 for $\varphi = 0.5$ and $\varphi = 0.2$ with $P_2 = P_1$ and $h = 0$, respectively, which mean that in Figure 6, R is placed on the middle of the straight line S_1-to-S_2, and in Figure 7, R is closer to S_1 than S_2.

From Figure 6, it can be observed that the optimal system outage probabilities of the five scenarios as shown in Table 2 decrease as the increment of P_1, and the system outage performance of the 1st scenario is much higher than that of the other four scenarios, which demonstrates that jointly optimizing the flexible power splitting factor and time assignment factor is superior to only optimizing the fixed power splitting factor and time assignment factor. The curves of the 2nd and the 4th scenarios are almost coincident with each other by only optimizing the power splitting factor ρ_i with fixed time assignment factor $\theta_i = 1/3$. And the curves of the 3rd and the 5th scenarios are also almost coincident with each other with jointly optimizing the power splitting factor ρ_i and the time assignment factor θ_i. But the system outage performances of the 3rd and the 5th scenarios outperform that of the 2nd and the 4th scenarios. In other words, the system outage performance obtained by jointly optimizing the power splitting factor ρ_i and the time assignment factor θ_i is better than by only optimizing the power splitting factor ρ_i with fixed time assignment factor $\theta_i = 1/3$, or the time assignment factor θ_i can greatly affect the system outage performance with jointly optimizing the power splitting factor ρ_i.

The similar results can also be seen in Figure 7, but the curves of the 3rd and the 5th scenarios are close to each other when P_1 is within the interval of 0 dBm to 25 dBm and almost coincident when P_1 goes to the rest of the value, because more harvested energy should be allocated to P_1 in order to reduce the growing path loss firstly with $\varphi = 0.2$, and then P_1 is large enough to meet the system requirements. Besides, the system outage performance gain between the 3rd, 5th scenarios and the 2nd, 4th scenarios is larger than that in Figure 6, which mean that no matter whether R is placed in the middle position of S_1 and S_2 or not, jointly optimizing the power splitting factor ρ_i and the time assignment factor θ_i on the system outage performance outperforms only optimizing the power splitting factor ρ_i with the fixed time assignment factor $\theta_i = 1/3$. Thus, depending on those different influences, we can reasonably configure system parameters in practice.

Figure 8 shows the system outage probability versus P_1 and φ for PS-TWR based on the 5th scenario as shown in Table 2, where it shows that the system outage probability achieves its minimum at R deployed closer to source nodes with better channel quality. Figure 9 plots the optimal region of P_1 and φ for system outage probability, which may guide us to select a proper P_1 and φ pair to obtain the optimal system outage probability.

7.3. Effect of Relay Location on System Outage Probability. In this subsection, we shall discuss the system performances of PS-TWR and TS-TWR by varying the location of R with different h. As shown in Figure 4, the relay location is described by the ratio φ changing in $(0, 1)$, so that we set it

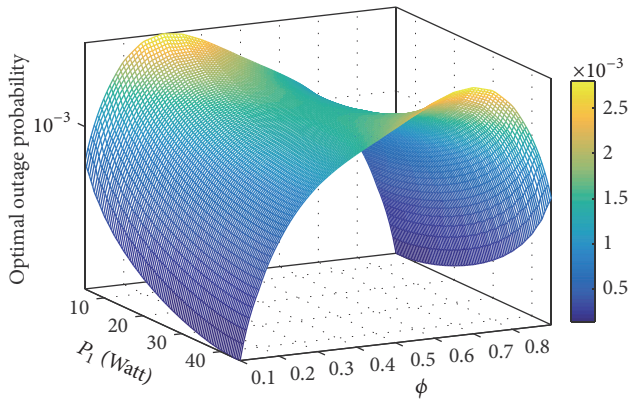

FIGURE 8: Three-dimensional graph of system outage probability for PS-TWR with $P_2 = 50 - P_1$, $h = 0$, and $d_{S,S} = 100$ m.

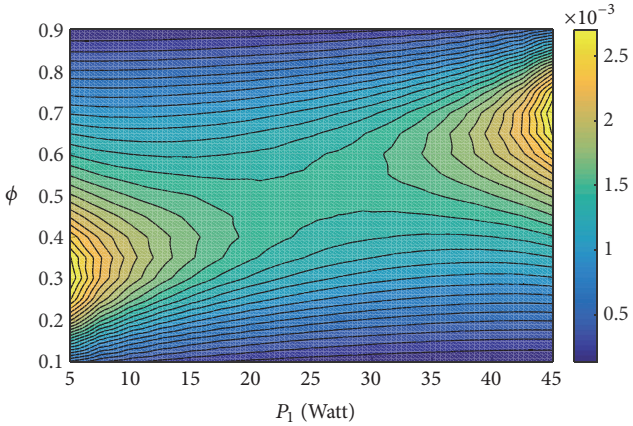

FIGURE 9: Optimal region of P_1 and φ for system outage probability with $P_2 = 50 - P_1$, $h = 0$, and $d_{S,S} = 100$ m for PS-TWR.

varies from 0.1 to 0.9 with $h = 0$ and $h = 50$ m in Figures 10 and 11, respectively.

From Figure 10, we can see that the optimal system outage probabilities of the five scenarios as shown in Table 2 first increase and then decrease with the increment of φ and achieve their maximums at $\varphi = 0.5$, that is, when R is positioned on the middle of the direct link S_1-to-S_2. It is noteworthy that the system outage probability is differ from the traditional case where EH is not considered at the relay and the minimal outage probability is achieved when R is deployed in the middle of S_i and S_2.

While, in Figure 11, the system outage probabilities of the five scenarios first decrease and then increase with the increment of φ and achieve their minimums at $\varphi = 0.5$, these results are opposite to that in Figure 10 but similar to the traditional case. The reason may be that when φ is small, R is closer to S_1, a higher energy harvesting efficiency can be yielded at R from S_1 and S_2. When φ is 0.5, R is placed on the middle of the direct link S_i-to-S_2 and now lower energy harvesting efficiency can be obtained at R, which may have effect on the system outage problem. When φ is large, R is closer to S_2, which leading to the result is opposite for the

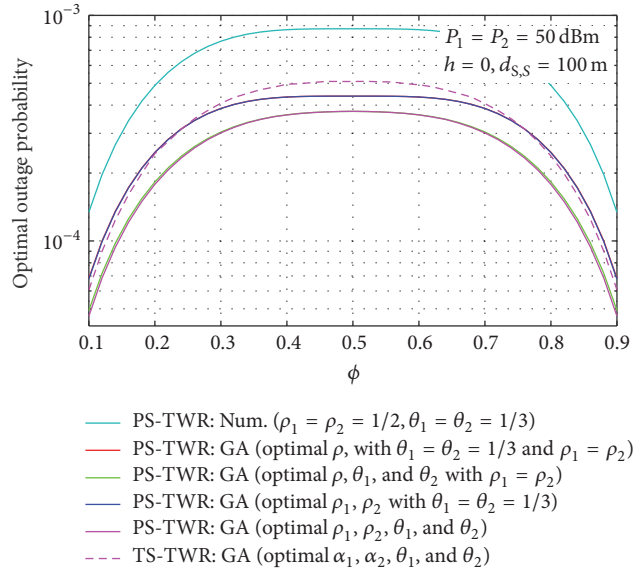

FIGURE 10: System outage probability versus φ with $h = 0$, $d_{S,S} = 100$ m, and $P_1 = P_2 = 50$ dBm.

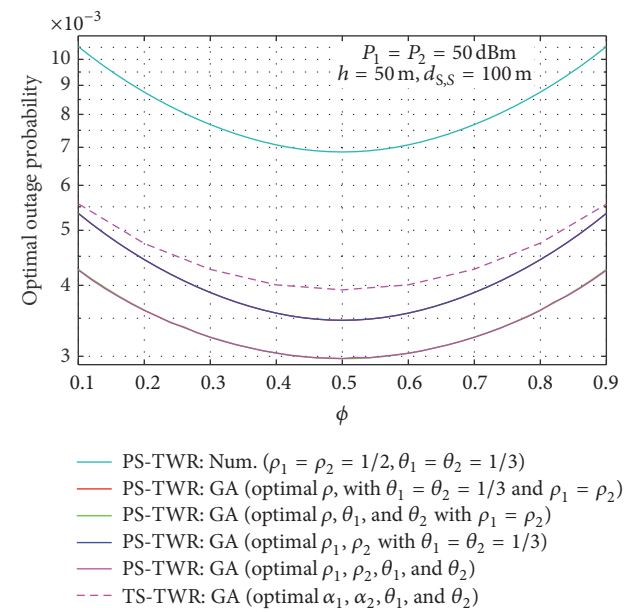

FIGURE 11: System outage probability versus φ with $h = 50$, $d_{S,S} = 100$ m, and $P_1 = P_2 = 50$ dBm.

symmetric channel model. Besides, from Figures 10 and 11, we can also find that PS-TWR can greatly improve the system outage performance compared with TS-TWR.

To further investigate the effect of the relay location on the system outage performance, we set the height h to be 0 m and 100 m, and the distance ratio φ to vary from 0.1 to 0.9. Figure 12 plots the system outage probability when $P_1 = P_2 = 50$ dBm and $d_{S,S} = 100$ m. It can be observed that, as h increasing, the optimal outage probability is significantly different. The curve of the optimal system outage probability is convex when h varies from 0 m to 40 m. However, when

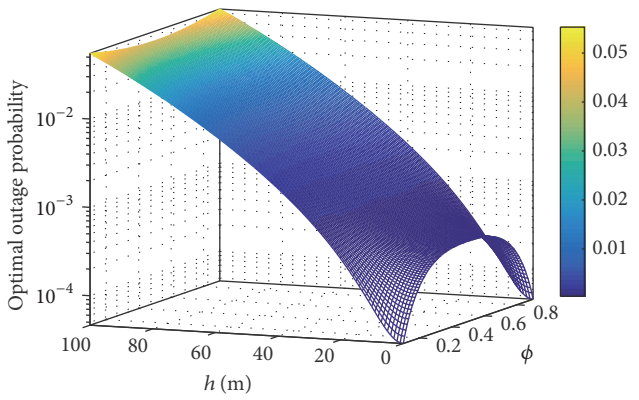

Figure 12: Three-dimensional graph of system outage probability for PS-TWR with $P_1 = P_2 = 50$ dBm and $d_{S,S} = 100$ m.

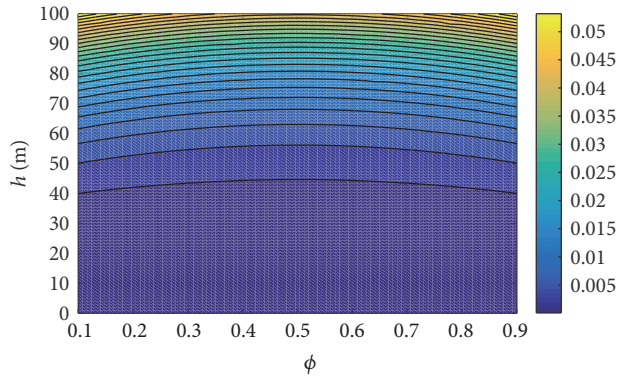

Figure 13: Optimal region of P_1 and φ for system outage probability with $P_1 = P_2 = 50$ dBm and $d_{S,S} = 100$ m for PS-TWR.

h changes in $(40, 100)$, the curve is concave. As a result, the maximum outage probability is achieved when the relay is deployed in the middle of the two sources with h changing in $(0, 40)$ as shown in Figure 10, so that, in order to make the system outage performance better, the relay node should be deployed closer to the source node with better channel quality, whereas, when h changes in $(40, 100)$, the result is exactly the opposite when h changes in $(0, 40)$ as shown in Figure 11.

Besides, Figure 13 plots the optimal region of the relay location versus P_1 and φ for system outage probability corresponding to Figure 12, where the obtained results may guide us to select a suitable location for the relay to achieve the optimal outage probability.

7.4. Convergence Behavior of GA-Based Algorithm. Figure 14 plots the convergence behaviors of the system outage probability by using the GA-based algorithm during 25 generations from the 2nd to the 5th scenarios as shown in Table 2. It can been seen that since the number of optimized parameters is different, the curve of the 5th scenario converges slower than the other three scenarios. For the 2nd and 4th scenarios, the convergence point is found within 5 runs, and the predefined

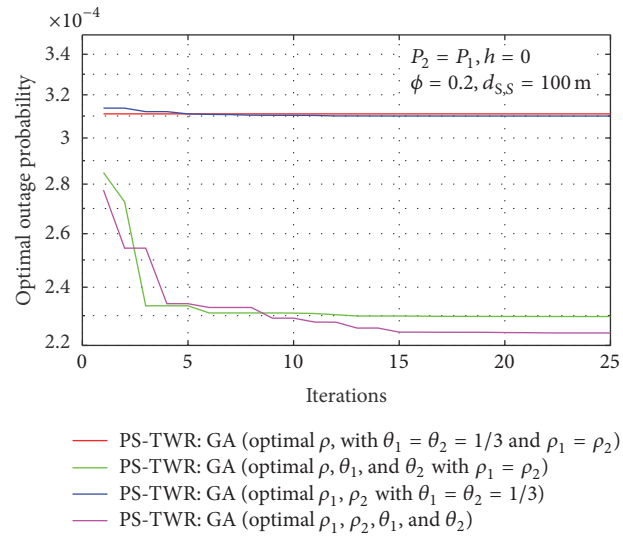

Figure 14: Convergence behavior of GA-based algorithm.

precision of the 3rd and the 5th scenarios is achieved after almost 15 generations.

7.5. Comparison of the Exact and the Approximate Outage Probabilities. The approximate versus the theoretical analysis system outage probabilities based on the 5th scenario as shown in Table 2 for PS-TWR and Table 3 for TS-TWR are plotted in Figures 15(a) and 15(b), respectively. It can be seen that all approximate outage probability results obtained by our analytical expressions in Theorems 2, 3, 5, and 6 are very close to those of the exact ones obtained in Theorems 1 and 4, respectively, which validate our analytical results for the approximate outage operability of PS-TWR and TS-TWR.

8. Conclusion

This paper investigated SWIPT in a network-coded two-way relay system with exploring the system outage performance. For such a system, we presented two protocols, PS-TWR and TS-TWR to analyze the system outage performance. Besides, we also derived the corresponding approximate expressions of the system outage probability at the high and low SNR regions, respectively. In order to explore effects of the relay position and the sources transmit power on the system outage performance, we formulated two optimization problems to minimize the system outage probability by jointly optimizing the power splitting factor of the energy harvesting receiver and the time assignment factor of transmission phase for PS-TWR, and by jointly optimizing the time splitting factor of the energy harvesting receiver and the time assignment factor of transmission phase for TS-TWR. To solve the problems, we designed GA-based algorithm for them. Numerical and simulation results validated our theoretical analysis. It is shown that by jointly optimizing the time assignment and the SWIPT receiver parameters, a great performance gain can be achieved for both PS-TWR and TS-TWR. It is also shown that the optimized PS-TWR always outperforms the

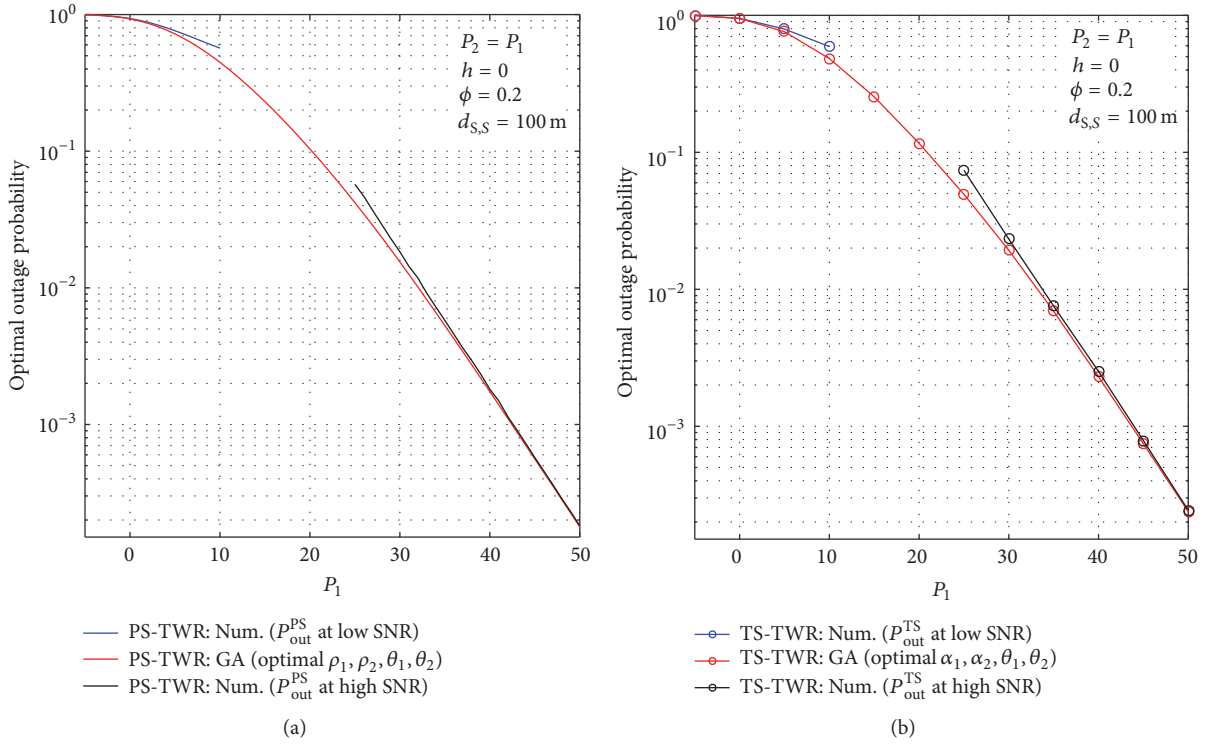

FIGURE 15: (a) Approximate outage probability for PS-TW. (b) Approximate outage probability for TS-TWR.

optimized TS-TWR in terms of outage performance. In addition, the effects of various system parameters including the relay location, the transmit power of the two sources are also discussed, which provide some insights for the SWIPT-enabled two-way relay networks.

Appendix

Proof of Theorem 1

This appendix gives the derivative of P_{out}^{PS} in (11) for PS-TWR. Substituting (3), (5), and (8) into (9), we can obtain that

$$P_{out}^{(PS)} = 1 - \Pr\left[|h_1|^2 \geq c\right] \Pr\left[|h_2|^2 \geq d\right] \times \Pr\left[w \geq \frac{u_3}{a|h_1|^2 + b|h_2|^2}\right], \tag{A.1}$$

where

$$a = \frac{\theta_1}{(1-\theta_1-\theta_2)} \zeta \rho_1 P_1 d_{S,1}^{-m},$$

$$b = \frac{\theta_2}{(1-\theta_1-\theta_2)} \zeta \rho_2 P_2 d_{S,2}^{-m},$$

$$c = \frac{u_1 d_{S,1}^m \sigma_{R,1}^2}{(1-\rho_1) P_1},$$

$$d = \frac{u_2 d_{S,2}^m \sigma_{R,2}^2}{(1-\rho_2) P_2},$$

$$u_1 = 2^{(1/\theta_1)R_{sr}} - 1,$$

$$u_2 = 2^{(1/\theta_2)R_{sr}} - 1,$$

$$u_3 = 2^{(1/(1-\theta_1-\theta_2))R_{sr}} - 1,$$

$$w = \min\left(\frac{|f_1|^2}{d_{S,1}^m \sigma_{S,1}^2}, \frac{|f_2|^2}{d_{S,2}^m \sigma_{S,2}^2}\right). \tag{A.2}$$

Since $|h_i|^2$ is exponential random variable with mean λ_{h_i}, we can obtain that

$$\Pr\left[R_{S,1}^{(PS)} \geq R_{sr}\right] = e^{-\lambda_{h_1} c},$$
$$\Pr\left[R_{S,2}^{(PS)} \geq R_{sr}\right] = e^{-\lambda_{h_2} d}. \tag{A.3}$$

Setting $t = a|h_1|^2 + b|h_2|^2$, the probability density function (PDF) of t can be written as

$$f_t(t) = \begin{cases} \dfrac{\lambda_{h_1}\lambda_{h_2}}{a\lambda_{h_2} - b\lambda_{h_1}} \left(e^{-(\lambda_{h_1}/a)t} - e^{-(\lambda_{h_2}/b)t}\right), & a\lambda_{h_2} \neq b\lambda_{h_1}, \\ \dfrac{\lambda_{h_1}\lambda_{h_2}}{ab} e^{-(\lambda_{h_2}/b)t} \cdot t, & a\lambda_{h_2} = b\lambda_{h_1}. \end{cases} \tag{A.4}$$

And, the cumulative distribution function (CDF) of t can be given by

$$F_t(t) = 1 - e^{-(d_{S,1}^m \sigma_{S,1}^2 \lambda_{f_1} + d_{S,2}^m \sigma_{S,2}^2 \lambda_{f_2})t}. \tag{A.5}$$

At last, we can obtain (A.6) by applying the formula: $\int_0^\infty x^{v-1}\exp(-\beta/x-\gamma x)dx = 2(\beta/\gamma)^{v/2}K_v(2\sqrt{\beta\gamma})$ [36].

$$\Pr\left[t \geq \frac{u_3}{a\left|h_1\right|^2 + b\left|h_2\right|^2}\right] = \int_0^\infty e^{-(d_{S,1}^m \sigma_{S,1}^2 \lambda_{f_1} + d_{S,2}^m \sigma_{S,2}^2 \lambda_{f_2}) u_3/t} \cdot f_t(t)\, dt$$

$$= \begin{cases} \dfrac{2\lambda_{h_1}\lambda_{h_2}}{a\lambda_{h_2} - b\lambda_{h_1}} \left(\sqrt{\dfrac{z_0 u_3 a}{\lambda_{h_1}}} K_1\left(2\sqrt{\dfrac{z_0 u_3 \lambda_{h_1}}{a}}\right) - \sqrt{\dfrac{z_0 u_3 b}{\lambda_{h_2}}} K_1\left(2\sqrt{\dfrac{z_0 u_3 \lambda_{h_2}}{b}}\right)\right), & a\lambda_{h_2} \neq b\lambda_{h_1}, \\ \dfrac{2\lambda_{h_1} z_0 u_3}{a} K_2\left(2\sqrt{\dfrac{z_0 u_3 \lambda_{h_2}}{b}}\right), & a\lambda_{h_2} = b\lambda_{h_1}, \end{cases} \tag{A.6}$$

where $z_0 = d_{S,1}^m \sigma_{S,1}^2 \lambda_{f_1} + d_{S,2}^m \sigma_{S,2}^2 \lambda_{f_2}$ and $K_1(\cdot)$ and $K_2(\cdot)$ denote the first-order and second-order modified Bessel functions of the second kind, respectively.

Substituting (A.3) and (A.6) into (A.1), (11) can be obtained. Therefore, Theorem 1 is proved.

Competing Interests

The authors declare that there is no conflict of interests regarding the publication of this paper.

Acknowledgments

This work was supported by the National Natural Science Foundation of China (no. 61671051 and no. 61602034), by Beijing Natural Science Foundation (no. 4162049), by the Open Research Fund of National Mobile Communications Research Laboratory, Southeast University (no. 2014D03), and also by the Fundamental Research Funds for the Central Universities of Beijing Jiaotong University (no. 2016JBM015).

References

[1] D.-T. Do, "Time power switching based relaying protocol in energy harvesting mobile node: optimal throughput analysis," *Mobile Information Systems*, vol. 2015, Article ID 769286, 8 pages, 2015.

[2] A. Bakkali, J. Pelegri-Sebastia, T. Sogorb, V. Llario, and A. Bou-Escriva, "A Dual-band antenna for RF energy harvesting systems in wireless sensor networks," *Journal of Sensors*, vol. 2016, Article ID 5725836, 8 pages, 2016.

[3] Y. F. Hu, N. Cao, and Y. F. Chen, "Analysis of wireless energy harvesting relay throughput in rician channel," *Mobile Information Systems*, vol. 2016, Article ID 8798494, 9 pages, 2016.

[4] D. Yang, C. Zhu, L. Xiao, X. Shen, and T. Zhang, "An energy-efficient scheme for multirelay cooperative networks with energy harvesting," *Mobile Information Systems*, vol. 2016, Article ID 5618935, 10 pages, 2016.

[5] F. Hu, B. Chen, X. Zhai, and C. Zhu, "Channel Selection Policy in Multi-SU and Multi-PU Cognitive Radio Networks with Energy Harvesting for Internet of Everything," *Mobile Information Systems*, vol. 2016, Article ID 6024928, 12 pages, 2016.

[6] G. Du, K. Xiong, and Z. Qiu, "Outage analysis of cooperative transmission with energy harvesting relay: time switching versus power splitting," *Mathematical Problems in Engineering*, vol. 2015, Article ID 598290, 9 pages, 2015.

[7] K. Vijayaraghavan and R. Rajamani, "Novel batteryless wireless sensor for traffic-flow measurement," *IEEE Transactions on Vehicular Technology*, vol. 59, no. 7, pp. 3249–3260, 2010.

[8] C. Huang, R. Zhang, and S. Cui, "Throughput maximization for the gaussian relay channel with energy harvesting constraints," *IEEE Journal on Selected Areas in Communications*, vol. 31, no. 8, pp. 1469–1479, 2013.

[9] D. T. Hoang, D. Niyato, P. Wang, and D. I. Kim, "Performance optimization for cooperative multiuser cognitive radio networks with RF energy harvesting capability," *IEEE Transactions on Wireless Communications*, vol. 14, no. 7, pp. 3614–3629, 2015.

[10] V. Raghunathan, S. Ganeriwal, and M. Srivastava, "Emerging techniques for long lived wireless sensor networks," *IEEE Communications Magazine*, vol. 44, no. 4, pp. 108–114, 2006.

[11] K. Tutuncuoglu and A. Yener, "Optimum transmission policies for battery limited energy harvesting nodes," *IEEE Transactions on Wireless Communications*, vol. 11, no. 3, pp. 1180–1189, 2012.

[12] L. R. Varshney, "Transporting information and energy simultaneously," in *Proceedings of the IEEE International Symposium on Information Theory (ISIT '08)*, pp. 1612–1616, IEEE, July 2008.

[13] Y. Yao, C. Yin, and S. Huang, "Throughput characterization for cooperative wireless information transmission with RF energy harvesting-based relay," *Mobile Information Systems*, vol. 2016, Article ID 8907267, 11 pages, 2016.

[14] X. Zhou, R. Zhang, and C. K. Ho, "Wireless information and power transfer: architecture design and rate-energy tradeoff," *IEEE Transactions on Communications*, vol. 61, no. 11, pp. 4754–4767, 2013.

[15] X. Zhou, "Training-based SWIPT: optimal power splitting at the receiver," *IEEE Transactions on Vehicular Technology*, vol. 64, no. 9, pp. 4377–4382, 2015.

[16] P. Popovski, A. M. Fouladgar, and O. Simeone, "Interactive joint transfer of energy and information," *IEEE Transactions on Communications*, vol. 61, no. 5, pp. 2086–2097, 2013.

[17] A. Ortiz, H. Al-Shatri, X. Li, T. Weber, and A. Klein, "Throughput maximization in two-hop energy harvesting communications," in *Proceedings of the International Symposium on Wireless Communication Systems (ISWCS '15)*, pp. 291–295, IEEE, Brussels, Belgium, August 2015.

[18] R. Zhang and C. K. Ho, "MIMO broadcasting for simultaneous wireless information and power transfer," *IEEE Transactions on Wireless Communications*, vol. 12, no. 5, pp. 1989–2001, 2013.

[19] K. Xiong, P. Fan, C. Zhang, and K. B. Letaief, "Wireless information and energy transfer for two-hop non-regenerative MIMO-OFDM relay networks," *IEEE Journal on Selected Areas in Communications*, vol. 33, no. 8, pp. 1595–1611, 2015.

[20] I. Krikidis, S. Timotheou, and S. Sasaki, "RF energy transfer for cooperative networks: data relaying or energy harvesting?" *IEEE Communications Letters*, vol. 16, no. 11, pp. 1772–1775, 2012.

[21] A. A. Nasir, X. Zhou, S. Durrani, and R. A. Kennedy, "Relaying protocols for wireless energy harvesting and information processing," *IEEE Transactions on Wireless Communications*, vol. 12, no. 7, pp. 3622–3636, 2013.

[22] X. Di, K. Xiong, Y. Zhang, and Z. Qiu, "Simultaneous wireless information and power transfer in two-hop OFDM decode-and-forward relay networks," *KSII Transactions on Internet and Information Systems*, vol. 10, no. 1, pp. 152–167, 2016.

[23] Z. Hadzi-Velkov, N. Zlatanov, T. Q. Duong, and R. Schober, "Rate maximization of decode-and-forward relaying systems with RF energy harvesting," *IEEE Communications Letters*, vol. 19, no. 12, pp. 2290–2293, 2015.

[24] C. Huang, P. Sadeghi, and A. A. Nasir, "BER performance analysis and optimization for energy harvesting two-way relay networks," in *Proceedings of the Australian Communications Theory Workshop (AusCTW '16)*, pp. 65–70, IEEE, Melbourne, Australia, January 2016.

[25] J. Men, J. Ge, C. Zhang, and J. Li, "Joint optimal power allocation and relay selection scheme in energy harvesting asymmetric two-way relaying system," *IET Communications*, vol. 9, no. 11, pp. 1421–1426, 2015.

[26] G. Y. Du, K. Xiong, Y. Zhang, and Z. D. Qiu, "Outage analysis and optimization for four-phase two-way transmission with energy harvesting relay," *KSII Transactions on Internet and Information Systems*, vol. 8, no. 10, pp. 3321–3341, 2014.

[27] X. Di, K. Xiong, P. Fan, and H.-C. Yang, "Simultaneous wireless information and power transfer in cooperative relay networks with rateless codes," *IEEE Transactions on Vehicular Technology*, 2016.

[28] G. Du, K. Xiong, Y. Zhang, and Z. Qiu, "Outage analysis and optimization for time switching-based two-way relaying with energy harvesting relay node," *KSII Transactions on Internet and Information Systems*, vol. 9, no. 2, pp. 545–563, 2015.

[29] K. Xiong, P. Fan, K. Ben Letaief, S. Yi, and M. Lei, "Resource allocation for minimal downlink delay in two-way OFDM relaying with network coding," in *Proceedings of the IEEE International Conference on Communications (ICC '12)*, pp. 5343–5347, IEEE, Ottawa, Canada, June 2012.

[30] Q. You, Y. Li, and Z. Chen, "Joint relay selection and network coding for error-prone two-way decode-and-forward relay networks," *IEEE Transactions on Communications*, vol. 62, no. 10, pp. 3420–3433, 2014.

[31] J. Rostampoor and S. M. Razavizadeh, "Energy efficiency and sum-rate maximization in MIMO two-way relay networks," in *Proceedings of the 23rd Iranian Conference on Electrical Engineering (ICEE '15)*, pp. 528–533, IEEE, Tehran, Iran, May 2015.

[32] K. Xiong, P. Fan, T. Li, and K. B. Letaief, "Outage probability of space-time network coding over rayleigh fading channels," *IEEE Transactions on Vehicular Technology*, vol. 63, no. 4, pp. 1965–1970, 2014.

[33] K. Xiong, P. Fan, H.-C. Yang, and K. B. Letaief, "Space-time network coding with overhearing relays," *IEEE Transactions on Wireless Communications*, vol. 13, no. 7, pp. 3567–3582, 2014.

[34] M. Abramowitz and I. A. Stegun, *Handbook of Mathematical Functions, with Formulas, Graphs, and Mathematical Tables*, Dover, New York, NY, USA, 1972.

[35] K. F. Man, K. S. Tang, and S. Kwong, "Genetic algorithms: concepts and applications," *IEEE Transactions on Industrial Electronics*, vol. 43, no. 5, pp. 519–534, 1996.

[36] I. S. Gradshteyn and I. M. Ryzhik, *Table of Integrals, Series, and Products*, Academic Press, 4th edition, 1980.